

Marcelo Barreiro · Ping Chang · R. Saravanan

Simulated precipitation response to SST forcing and potential predictability in the region of the South Atlantic convergence zone

Received: 28 June 2004 / Accepted: 22 October 2004 / Published online: 9 December 2004
© Springer-Verlag 2004

Abstract The sensitivity of the precipitation response in the South Atlantic convergence zone (SACZ) to sea surface temperature (SST) anomaly is investigated by an inter-model comparison study of ensembles of multi-decadal integrations of two atmospheric general circulation models (AGCMs)—version 1 of the NASA Seasonal-to-Interannual Prediction Project (NSIPP-1) model, and the NCAR community climate model (CCM3) version 3.6.6. Despite the different physical parameterizations, the two models consistently show an SST-forced signal located mainly over the oceanic portion of the SACZ. The signal has interannual-to-decadal timescales, and consists of a shift and strengthening of the SACZ toward anomalous warm waters. A potential predictability analysis reveals that the maximum predictable variance is about 50% of the total SACZ variance over the ocean, but the signal attenuates rapidly toward the South American continent. This result implies that the land portion of the SACZ is primarily dominated by the internal variability, thereby having a limited potential predictability at seasonal timescales.

Forced atmospheric variability due to anomalous sea surface temperatures (SST) gives rise to the possibility of seasonal climate forecasts to an otherwise chaotic system (e.g., Koster et al. 2000; Rowell 1998). Identifying areas of high potential predictability (“potential” meaning that the model is assumed perfect and the surface state of the ocean is known in advance), is therefore of great importance. Most of these areas are in the deep tropics, where SST forcing contributes predominantly to the low-frequency atmospheric variability, and the knowledge of ocean conditions allows the prediction of precipitation anomalies at least a season in advance (e.g., Goddard et al. 2001). In the extratropics, where atmospheric internal dynamics is the most important factor in determining its variability, precipitation anomalies cannot generally be predicted beyond the 1–2-week limit determined by chaotic dynamics. Additional predictability may come from atmospheric teleconnection patterns induced by tropical SST anomalies (like the Pacific-North American pattern). In the subtropics, areas where forced variability could potentially dominate are the subtropical convergence zones, such as the South Atlantic convergence zone (SACZ) and the South Pacific convergence zone. These are deep convective regions where the atmosphere is thought to be sensitive to changes in SST. In this work, we examine the variability of precipitation in the SACZ on interannual-to-decadal timescales.

The SACZ is a band of enhanced convective activity with rainfall rates larger than 4 mm day^{-1} that has its largest development during austral summer (January–February–March, hereafter JFM). It extends from the Amazon basin to the southeast subtropical and extratropical Atlantic ocean in a northwest–southeast line (Fig. 1a). The interannual variability of precipitation during JFM is of comparable magnitude as the seasonal mean with the maximum over the continent and extending southeastward toward the ocean (Fig. 1b).

Barreiro et al. (2002) (hereafter BCS) have studied the SST-forced variability of the SACZ during JFM in a

1 Introduction

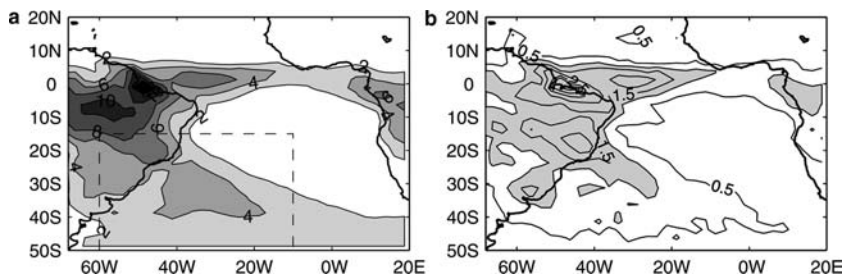
Understanding of precipitation variability and predictability has been a central focus in climate research.

M. Barreiro (✉)
Atmospheric and Oceanic Sciences Program,
Princeton University, Princeton, NJ 08544-0710, USA
E-mail: barreiro@princeton.edu

P. Chang
Department of Oceanography, Texas A&M University,
College Station, TX 77843-3186, USA

R. Saravanan
National Center for Atmospheric Research,
Boulder, CO 80307, USA

Fig. 1 **a** JFM precipitation climatology and **b** RMS deviation for observations (GPCP) during the period 1979–1994. Contour interval is 2 mm day^{-1} for climatology, and 0.5 mm day^{-1} for RMS deviation. The *dashed box* marks the SACZ region



five-member ensemble of AMIP-type simulations using version 3.6.6 of the community climate model (CCM3) developed at the National Center for Atmospheric Research (NCAR). A forced variability in the SACZ was detected with the aid of a signal-to-noise (S/N) optimization procedure. The signal varies on interannual-to-decadal timescales and consists of a dipole in precipitation with increased rainfall in the northern part of the SACZ and decreased rainfall to its southwest when SST anomalies are positive between the Equator and 30°S . The forced response attenuates rapidly toward land, where the SACZ variability was found to be dominated by internal variability. Robertson et al. (2003) report a similar atmospheric response to Atlantic SST anomalies.

Although the results of BCS show a limited potential predictability over the land area, these results may be sensitive to the physics of the model or to the ensemble size, and a further comparison with other models' output is highly desirable. In this follow-up study, we report on the reproducibility of the results found in BCS. We compare a larger ensemble of SST-forced CCM3 runs to an ensemble of similar runs made by version 1 of the AGCM developed at the NASA Seasonal-to-Interannual Prediction Project (NSIPP-1). Since both models contain different physical parameterizations and land-surface packages, we can test the robustness of the atmospheric response to SST anomalies in the SACZ found in BCS. We are particularly interested in the SST-forced precipitation anomaly over the continental part of the SACZ, because it is highly relevant to seasonal climate forecasting in a densely populated area. We shall re-examine the spatial structure of the predictable precipitation signal and quantify its strength during the peak season of the SACZ in both models.

Additionally, we will attempt to quantify the potential predictability of the SACZ region. Identifying a forced response does not necessarily translate into high predictability, because the strength of the signal may be weak compared to the strength of the noise. Therefore, it is very important to address the issue of whether the forced response is likely to dominate the dynamics or not. This can be accomplished by defining a potential predictability measure as the ratio of the signal variance over the total variance. We further calculate the modes of precipitation associated with internal variability. In this way, we can compare not only the ratio of forced versus total variability, but also the spatial structure of internal variability in the two models. Our results show

that the precipitation in the SACZ region is largely dominated by internal variability, and that the leading modes of simulated internal variability have structures similar to that of the leading mode of variability observed in the region (e.g., Robertson and Mechoso 2000).

The paper is organized as follows. In Sect. 2, we describe the data sets used, and compare the climatology and RMS deviation of the simulated SACZ with those of observations. In Sect. 3, we give a brief summary of the methodology used to extract a forced response in the models. In Sect. 4, we compare the variability in the SACZ region simulated by both AGCMs. In particular, we re-examine the findings of BCS, and compare the structure of the internal variability in the SACZ region in both models. In Sect. 5, we discuss the models' potential predictability for the precipitation. Finally, in Sect. 6, we summarize the major findings.

2 Data sets

The observational data set used in the study is that given by the Global Precipitation Climatology project (GPCP, Huffman et al. 1997), which is on a global $2.5^\circ \times 2.5^\circ$ grid and spans the time period 1979–2000.

We used the output of two AGCMs: the CCM3, which is a spectral model with T42 horizontal resolution (roughly $2.8^\circ \times 2.8^\circ$) and 19 vertical levels (Kiehl et al. 1998), and the NSIPP-1 model, which is a finite difference model with a resolution of $2.5^\circ \times 2^\circ$ with 17 levels in the vertical described in Bacmeister et al. (2000). The output of NSIPP-1 was regridded to a $2.5^\circ \times 2.5^\circ$ -grid to compare better with observations and with CCM3 output. Data for the NSIPP-1 model was obtained via the website <http://nsipp.gsfc.nasa.gov/main.html>. All analyses in this study are based on JFM seasonal averages. Statistical significance is computed using a two-sided Student's *t* test, assuming no year-to-year persistence.

A complete description of the models can be found in the references given. Here, we give a short description of the convective parameterization and land-surface schemes used in the models. The deep convective parameterization schemes used in both models are based on variants of the Arakawa–Schubert (AS) mass-flux scheme (Arakawa and Schubert (1974)). The CCM3 uses the scheme developed by Zhang and McFarlane (1995)

to account mainly for the effects of deep convection, and the scheme of Hack (1994) to deal with shallow and mid-level convection. The Zhang–McFarlane scheme assumes that the effects of convection are to relax the convective available potential energy (CAPE) towards a specified threshold value with a specified timescale. Quasi-equilibrium states develop when large-scale processes act to persistently increase local CAPE. The NSIPP-1 model uses the Relaxed-Arakawa-Schubert (RAS) scheme for penetrative convection originating in the boundary layer (Moorthy and Suarez 1992). The main difference between RAS and AS is that the state is “relaxed” toward equilibrium rather than requiring the final state to be balanced.

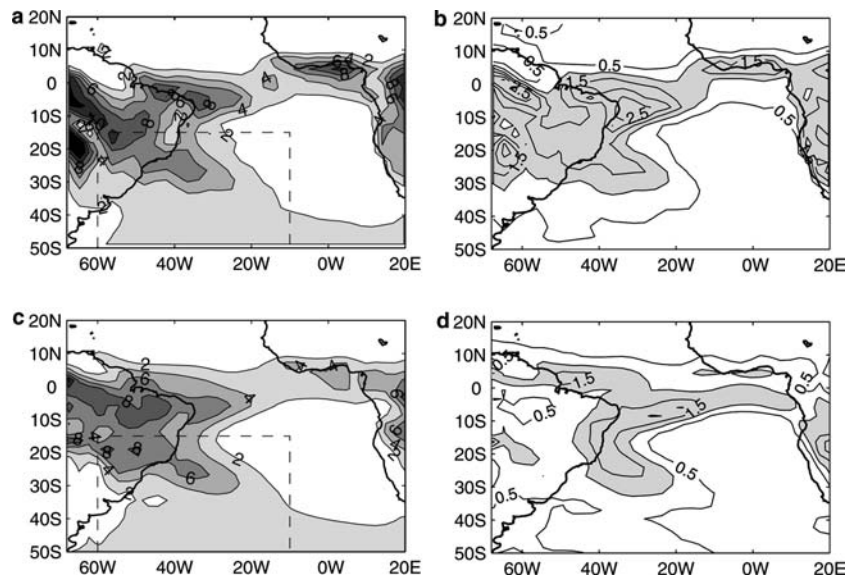
The land-surface model used in CCM3 is the NCAR LSM1.0, which is a one-dimensional model of energy, momentum, water and CO₂ exchange between the atmosphere and land. The model accounts for ecological differences among vegetation types, hydraulic and thermal differences among soil types, and allows for multiple surface types within a grid cell (Bonan 1998). The LSM used in NSIPP is a soil-vegetation-atmosphere transfer scheme called MOSAIC (Koster and Suarez 1996). MOSAIC subdivides each grid square into tiles of a single vegetation type and calculates separately one-dimensional energy and water balances over each tile with strong stomatal control over transpiration rates.

The models were run in the same experimental settings, forced with monthly global-observed SST as boundary conditions (commonly called GOGA-type of integrations, e.g., Chang et al. (2000)), and a nine-member ensemble was constructed for each model. The CCM3 integrations span the period 1950–1994, and were forced with the reconstructed SST of Smith et al. (1996). The NSIPP-1 integrations span the period 1930–2000, and the imposed SST (all with the same spatial resolution) were given by the Hadley Centre SST data set during 1930–1948, GISST 2.2 (Rayner et al. 1996)

during 1949–1981, and Reynolds Optimal Interpolation SST v1.0 during 1982–2000 (Reynolds and Smith 1994). As the three data sets have different climatologies, we calculated anomalies by removing the corresponding climatology in each of the periods. This procedure should not affect the results because we will not analyze interdecadal variability. The use of observed SST as a surface boundary condition for an AGCM implies an infinite heat capacity of the ocean. Some limitations of this approach have been noted, particularly in the extratropics (Saravanan 1998).

The modeled austral summer climatology of precipitation is shown in Fig. 2a, c. Both models simulate the mean position and magnitude of the SACZ well, although several differences with the observed SACZ can be noted. The connection of the SACZ with the Amazon convective region, apparent in the observations, is captured well in the CCM3 model, but is less clear in the NSIPP-1 model. Modeled precipitation also shows the separation between the rainfall bands associated with the SACZ and the intertropical convergence zone (ITCZ). However, contrary to observations, models tend to locate the ITCZ’s axis south of the equator, and overestimate rainfall next to the coast of Brazil at about 15°S, resulting in the undersizing of the south Atlantic dry zone. On the other hand, the simulated SACZ does not extend as far southeastward as the one observed. In observations, there is a clear discontinuity of the SACZ band near the coastline which hints the continental and oceanic parts of the SACZ do not vary as an integrated structure. This feature is also revealed well in the NSIPP-1 model, but is less obvious in the CCM3 model. The maximum precipitation in both models is over land, comparing well with observations, but they tend to overestimate rainfall intensity. The secondary precipitation maximum in the Andes at about (65°W–20°S) in the CCM3 is a bias of the model and has been previously noted (Hack et al. 1998).

Fig. 2 JFM precipitation climatology and RMS deviation during the period 1979–1994 for: **a, b** CCM3 model; **c, d** NSIPP-1 model. Contour interval is 2 mm day⁻¹ for climatology (*left*), and 0.5 mm day⁻¹ for RMS deviation (*right*). The *dashed boxes* mark the SACZ region



The CCM3 model captures the interannual variability of the SACZ with the maximum over the continent and extending southeastward over the ocean (Fig. 2b). The NSIPP-1 model, on the other hand, underestimates the precipitation variability over the continent and shows maximum variance over the oceanic portion of the SACZ (Fig. 2d). The origin of the underestimation of precipitation variance over land is uncertain, but is likely to depend on the parameterization of land-surface processes and their interaction with the atmosphere.

The SACZ has been shown to have large intraseasonal variations linked to the propagation of mid-latitude disturbances into the region (Liebmann et al. 1999), and to the Madden-Julian Oscillation (Paegle et al. 2000). Therefore, a good representation of the seasonal mean and its interannual variability depends, in part, on the correct simulation of these shorter timescale phenomena. Some of the differences between the simulated and the observed SACZ noted above may come from a deficient representation of these processes. Hence, a comparison of simulated intraseasonal variability in the CCM3 and NSIPP-1 with observations is desirable. Such an effort, however, represents a significant research project by its own and will not be the focus of this study. This study aims at understanding the mechanisms through which a local SST anomaly can force a precipitation response in the SACZ region on interannual timescales. We are mainly interested in the forced atmospheric response to the interannually varying SST, and this response can be considered to be separated from the intraseasonal variability, which comes from internal dynamics. Other authors have suggested that interannual and intraseasonal variability may be connected through the concept of weather regimes (e.g., Robertson et al. 2000). By intercomparing between different models, we expect the findings to be meaningful also in the real atmosphere even though the simulated and observed climates are not identical.

3 Detection of forced response

The methodology to extract a forced response is based on the so-called S/N optimization method used in BCS. This method is described in detail by Venzke et al. (1999). The basic assumption of the technique is that the time evolution of a model can be divided additively into two parts: an internal part (or noise), and an external part due to imposed boundary condition forcing (forced signal). In the models, the land surface interacts freely with the atmosphere. Thus, the internal part includes internal atmospheric variability as well as variability of the land surface and its effects on the atmosphere. The external part is due to SST forcing alone. The analysis decomposes the variability into a set of optimals according to the ratio of the S/N variance. In BCS, the first two optimals with maximum S/N variance ratio were considered as the forced signals. Here, we proceed

in a slightly different manner, which is perhaps more accurate and physically more sound: we first construct a total forced signal by summing up all the optimals that have an S/N-ratio larger than unity. The dominant forced pattern is then calculated as the first empirical orthogonal function (EOF) of the total signal variance. This method is preferred because the optimization method does not assure “a priori” that the first optimal is the pattern that explains the most signal variance. Theoretically, it may happen that the first optimal is a pattern that seldom occurs (then a small signal variance), but it is a pattern that is nearly orthogonal to the noise, thus giving a large S/N-ratio. By constructing the total signal variance and then performing an EOF analysis, we assure that the pattern is the one that explains most of the signal variance. The analysis below indicates that the first EOF of the total signal and the first optimal are in fact very similar in both spatial and temporal structures. The time series are highly correlated with a correlation coefficient r larger than 0.95 for the datasets we have considered.

Since the constructed signal is by definition common to all ensemble members, one can construct the noise part of the model evolution by subtracting the signal from each ensemble member. The spatial structure of the dominant internal mode can then be found by performing an EOF analysis on the noise variance. Here, we perform the EOF analysis over the concatenated noise parts of all ensemble members to enhance statistical significance. In sum, the S/N optimization technique adopted here allows for a better separation of signal and noise in a systematic way.

By comparing the relative strength of the signal (σ_s^2) and of the noise (σ_n^2) variance, one can also obtain an estimate of potential predictability. To do so, we define a potential predictability measure PP as the ratio between signal variance and total variance, i.e., $PP = \sigma_s^2 / (\sigma_s^2 + \sigma_n^2) = \sigma_s^2 / \sigma_t^2$, where σ_t^2 is the total variance. PP varies between 0 and 1, and the larger the value the more potentially predictable is the region. Note that the PP measure calculated here does not consider variability on intraseasonal timescales. The consideration of intraseasonal variability would increase the noise variance, but not likely the forced variance, therefore decreasing the value of PP .

Several approaches have been developed to measure potential predictability using an ensemble of climate simulations. Some approaches define a coherence index which “reflects the ability of the SST to guide the time sequencing of precipitation anomalies” (Koster et al. 2000), whereas others are based on “Analysis of Variance” (ANOVA) methods (e.g., Rowell 1998). Estimates of potential predictability have usually been of global extent, and have not focused on the SACZ region. Moreover, while ANOVA is a useful indicator of SST influence, it does not take into account correlations between grid points, and thus may lead to the erroneous conclusion that there are no SST effects. The measure of potential predictability used here

explicitly accounts for correlation between neighboring points, because it is constructed to represent the total signal as the sum of optimal structures calculated in the SACZ region. A weakness of the technique to estimate PP is that the construction of σ_s^2 , as mentioned above, depends on the truncation of the optimals. In this work, we used S/N-ratio larger than unity as a criteria for truncation. This choice of truncation is somewhat arbitrary and does not give a measure of the bias in the estimation of the total signal. This methodology of truncation may lead to an under or overestimation of the true signal. Thus, there is no obvious way to calculate the statistical significance of PP . To partially address this issue, we compare PP with the ANOVA estimate of potential predictability in which the significance level can be computed. We used a 1-way ANOVA model and calculated the adjusted coefficient of determination (see von Storch and Zwiers 1999).

4 Forced and internal precipitation variability

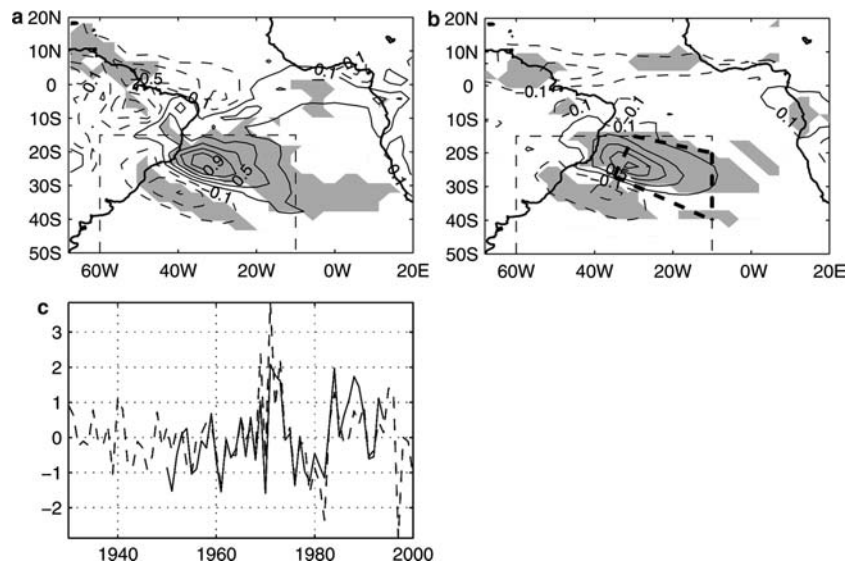
Analyses of models' output were performed over their respective time periods, that is, 1950–1994 for CCM3 and 1930–2000 for NSIPP-1. We consider a longer period for the NSIPP-1 model to use all the available data, and also because it overlaps the observational period. The use of NSIPP-1 data in the common period 1950–1994 does not change the main results of the study. Also, to isolate the SACZ from other features like the ITCZ with stronger variability, we performed the S/N optimization method in the region (60–10°W, 50–15°S) (box in Fig. 2, hereafter called the SACZ region). Analysis based on a larger area including the ITCZ and Amazon convection does not change the findings significantly, but makes it more difficult to isolate the variability in the SACZ region.

4.1 Forced signal

We applied the procedure described in Sect. 3 to the precipitation fields in the SACZ region. There is a striking similarity in structure and amplitude between the forced signals found in the CCM3 and NSIPP-1 models (Fig. 3a, b). The signals consist of a northwest–southeast-oriented dipole in precipitation anomalies mainly located off the coast of Brazil, as was found in BCS. The northern lobe of the dipole is stronger than the southern lobe, indicating a northward shift of the SACZ as well as a strengthening of rainfall in that region. The time series associated with the signals in the different models are shown in Fig. 3c. Both show interannual-to-decadal timescales and are correlated with $r=0.77$ over the common period 1950–1994, which is significant at the 99% level. Regression of the vertical velocity field at 500 mb in the NSIPP-1 model mimics the precipitation anomalies with anomalous ascent in areas of increased precipitation and descent over areas with negative precipitation anomalies (not shown). For the CCM3, vertical velocity fields were not available.

Regression of models' SST forcing onto corresponding time series reveal that the enhanced precipitation is located over warm SST anomaly with a maximum of roughly 0.45°C at about 20°S (see Fig. 4a, b). Also, the SST maps show that the warm SST anomalies tend to be accompanied by negative SST anomalies south of 30°S and north of the equator. The cross-equatorial SST gradient is consistent with the weakening and southward shift of the ITCZ seen in Fig. 3a, b. Regression of 1,000 mb winds shows a cyclonic eddy located over the same region off the coast of Brazil in both models, as well as northerly flow coming from the equatorial region into the SACZ (Fig. 4a, b). At upper levels, the anomaly shows anticyclonic circulation, consistent with a Gill-type baroclinic response (Gill 1980). Therefore, despite the different physical parameterizations, both GCMs

Fig. 3 Dominant forced signal of precipitation in the: **a** CCM3 model, and **b** NSIPP-1 model, shown as homogeneous regression maps. Contour interval is 0.2 mm day⁻¹, and shaded areas indicate significance at the 95% level using a two-sided t -test. The dashed box marks the region used to construct the precipitation index shown in Fig. 8. **c** Normalized time series of forced signal for CCM3 (solid line) and NSIPP-1 (dashed line)



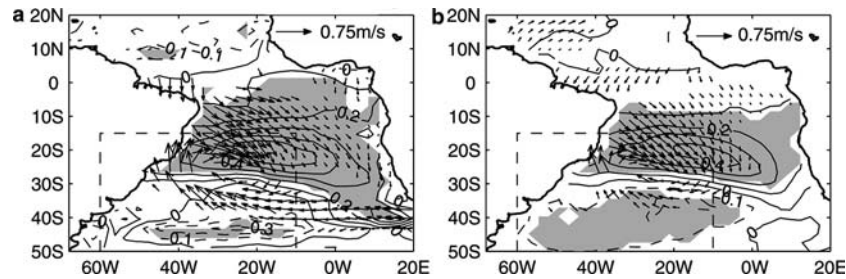


Fig. 4 Regression of 1,000 mb winds and SST anomalies onto the time series of the forced response in the **a** CCM3, and **b** NSIPP-1. Contour interval for the SST is 0.1 K. Shaded areas

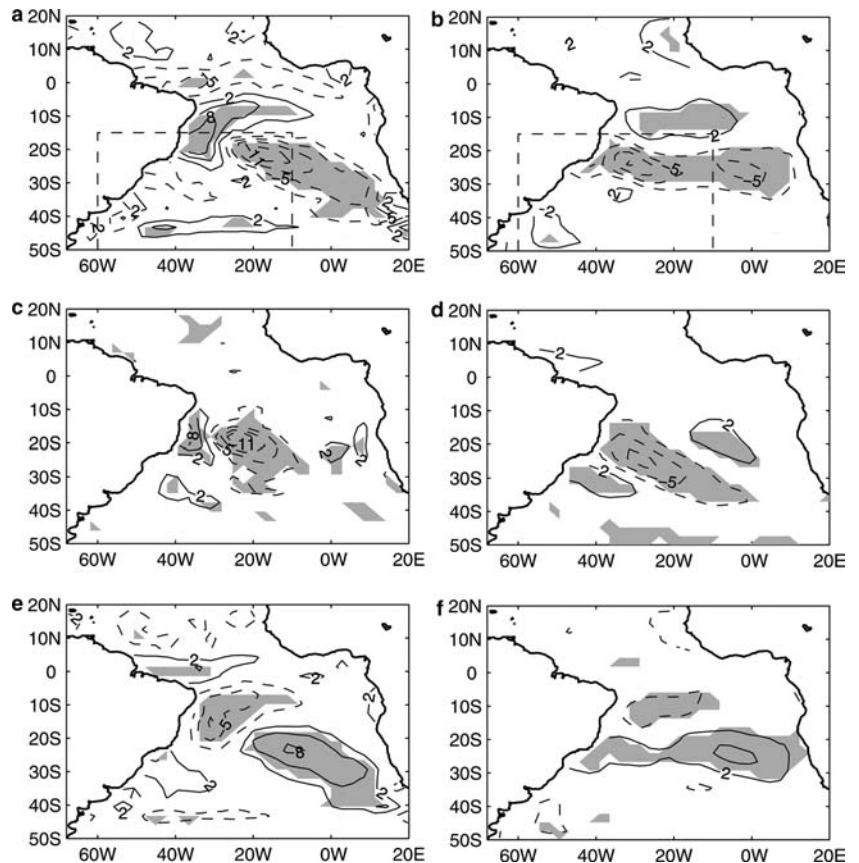
indicate SST anomalies significant at the 95% level. Only wind vectors, where the wind speed anomaly is significant at the 90% level, are plotted

present a forced response of the atmosphere very similar to local SST anomalies. The response pattern also agrees well with results of Robertson et al. (2003). Anomalies have larger amplitudes in the CCM3 in part because the regression for NSIPP-1 encompasses the period 1930–1960 in which the signal was relatively weak (see also Sect. 5). We suggest the following mechanism to explain the forced signal: a positive SST anomaly forces the atmosphere, generating a low-level hydrostatic cyclonic eddy next to the coast of South America. A northerly flow coming from equatorial regions, probably as a response to the tendency of having warmer SST anomalies to the south of the equator, is also present, which brings the enhanced moisture to the area. This anomalous

circulation creates a convergence in the northern part of the SACZ, causing an increase in precipitation. Compensating subsidence forms to its southwestern flank and creates a negative precipitation anomaly, which may be further reinforced by the low-moisture southerly flow.

Figure 5a, b shows the regression of the net heat flux into the ocean for both AGCMs. Heat-flux anomalies are generally stronger in the CCM3 model. Moreover, model responses differ in the SACZ region. At about (20°S, 35°W), the CCM3 presents a net heat-flux anomaly into the ocean coexisting with positive SST anomalies, suggesting a local positive air–sea feedback, which is not present in NSIPP-1 model. On the other hand, both models tend to suggest a positive feedback

Fig. 5 Regression of heat fluxes onto the time series of the forced response in the CCM3 (left) and NSIPP-1 (right) models. **a, b** net heat flux into the ocean; **c, d** downward solar radiation; **e, f** latent heat flux. Units are in W m^{-2} . Shaded areas as in Fig. 3. The boxes in (a), (b) mark the SACZ region



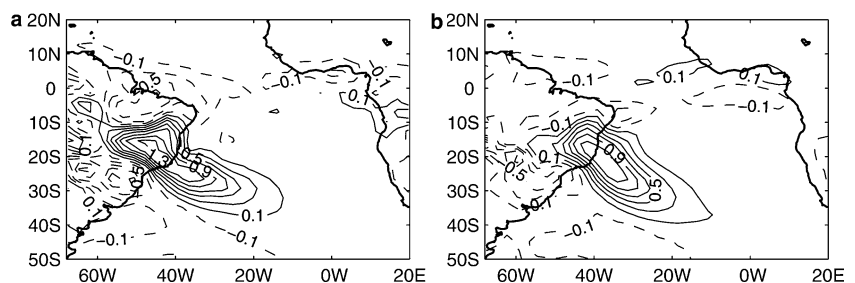
between heat fluxes and SST off the coast of Brazil at about 10°S (also found in BCS). There, the heat fluxes tend to maintain and shift the SST anomalies northward.

To investigate further we separated the net heat flux into four components: short-wave and long-wave radiation, and latent and sensible heat fluxes. In both models, the net heat flux ($Nhflx$) is approximately given by the difference between the downward solar radiation (Sw) and the latent heat flux ($Lhflx$), i.e., $Nhflx \approx Sw - Lhflx$. The NSIPP-1 model shows a negative anomaly of downward solar radiation at the same place of increased precipitation, suggesting that the presence of clouds shadows the surface, reducing the incoming energy and acting as a negative feedback (see Fig. 5d). To both sides of the negative anomaly, there are areas with increased solar radiation probably as a consequence of compensating subsidence which inhibits cloud formation. The CCM3 shows similar behavior in short-wave radiation except for a region of positive anomaly next to the coast of Brazil which indicates positive feedback (see Fig. 5c). The regression maps of the latent heat flux reveal that both models show negative anomaly next to the coast of Brazil at about 10°S. In the CCM3, however, the anomaly extends further south to 20°S contributing to the solar radiation anomaly to create the region of positive feedback in the SACZ region mentioned above (see Fig. 5e, f). The origin of these model differences is expected to be related to the different parameterizations of convection, of boundary layer processes, and of cloud–radiation interaction. Sensitivity experiments are needed to further investigate this result. East of 20°W, between 20–30°S both models show that latent heat flux tends to damp the SST anomalies. We further decomposed the latent heat-flux anomalies linearly into a component due to changes in the wind speed and a component due to changes in the air–sea gradient of specific humidity (see for example, Saravanan and Chang (2000)). We found that wind speed changes dominate the latent heat-flux anomaly in the region of positive feedback near the coast of Brazil. On the other hand, east of 20°W changes in the air–sea gradient of specific humidity dominates and damps the SST anomalies. This latter result is in agreement with Sterl and Hazeleger (2003), who found that while wind-induced latent heat flux helps creating the SST anomaly, changes in the air–sea gradient of specific humidity damp it.

4.2 Internal variability

In this section, we calculate the modes of precipitation associated with the interannual internal variability. The leading modes of precipitation in each model are found by performing an EOF analysis on the concatenated noise part variances, as described in Sect. 3. We consider only the first EOF of the noise for each model (hereafter called noise-EOF1) because it largely explains most of the noise variance in each model. Figure 6a, b shows the patterns of the noise-EOF1 for each model as a regression over a larger area. They explain 25 and 32% of total noise variance in the CCM3 and NSIPP-1 models, respectively. The structures of the noise-EOF1 in both models are similar, mainly showing an enhanced SACZ accompanied by decreased precipitation to its southwest as a consequence of compensating subsidence. There is also decreased precipitation in the ITCZ. Compared with the forced responses, the noise patterns show much larger weight over the land. One notable difference between the noise structures is that, in the CCM3 the maximum variance is over the continent, while in the NSIPP-1 the maximum is mainly located over the oceanic part of the SACZ. This difference in structure mimics differences in maps of RMS deviation (Fig. 2b, d). The surface wind anomaly accompanying the noise-EOF1 consists of an isolated eddy-like cyclonic structure located at $\approx (35^\circ\text{W}, 27^\circ\text{S})$ with a half-wavelength of about 40° in both longitude and latitude (not shown). Overall, the patterns shown in Fig. 6 have the same characteristics as the pattern of vertical velocity associated with the leading mode of interannual variability observed in the SACZ region found in Robertson and Mechoso (2000). They also found that this mode is largely due to internal variability of the atmosphere, which agrees with our findings, and that its associated time series contains a periodic component of 15–17 years. The time series of the noise-EOF1s, however, have very large intra-ensemble variability, showing almost no significant correlation between time series of different ensemble members (as expected for noise). Thus, it suggests that the leading noise patterns have no preferred timescale. The EOF technique used in Robertson and Mechoso (2000) is not designed to separate forced from internal variability, but to maximize explained variance. Thus, largely due to internal variability, their mode will likely also include a contribution from forced

Fig. 6 Dominant mode of internal variability for precipitation (noise-EOFs) in **a** CCM3, and **b** NSIPP-1 models. Contour interval is 0.2 mm day^{-1}



variability, which may explain the significant periodic component in the associated time series.

5 Potential predictability analysis

The previous sections have focused on the spatial and temporal characteristics of the forced and internal variability of the precipitation in the SACZ region. In this section, we investigate the issue of how predictable the precipitation is, and where the predictable region lies, assuming that SST is known in advance. This is done by using the potential predictability measure PP defined in Sect. 3. Furthermore, the map of the PP index is contrasted with the estimation of potential predictability given by a 1-way ANOVA model.

Figure 7a, b shows the potential predictability measure PP for each model. Overall, both models agree in that the variance of the predictable signal explains less than 10% of the total variance over the continent, and that it is significantly larger over the oceanic portion of the SACZ, mainly to the north of the SACZ's climatological axis. However, the potential predictability in the CCM3 model is larger than in the NSIPP-1 model in spite of the fact that the forced signals in both models are of about the same amplitude (see Fig. 3). This is also true when considering the NSIPP-1 output during the period 1950–1994, although PP increases. The reason is related to the structure of the noise in the models. In CCM3, the noise-EOF1 has the largest variability over the land and not so strong over the ocean. In the NSIPP-1 model, on the other hand, the noise-EOF1 has the largest loading over the oceanic part of the SACZ thus hindering the forced response.

Estimates of potential predictability given by ANOVA are very consistent with those of the PP index (Fig. 7c, d). They also tend to agree with the results of Rowell (1998) and of Koster et al. (2000) despite the

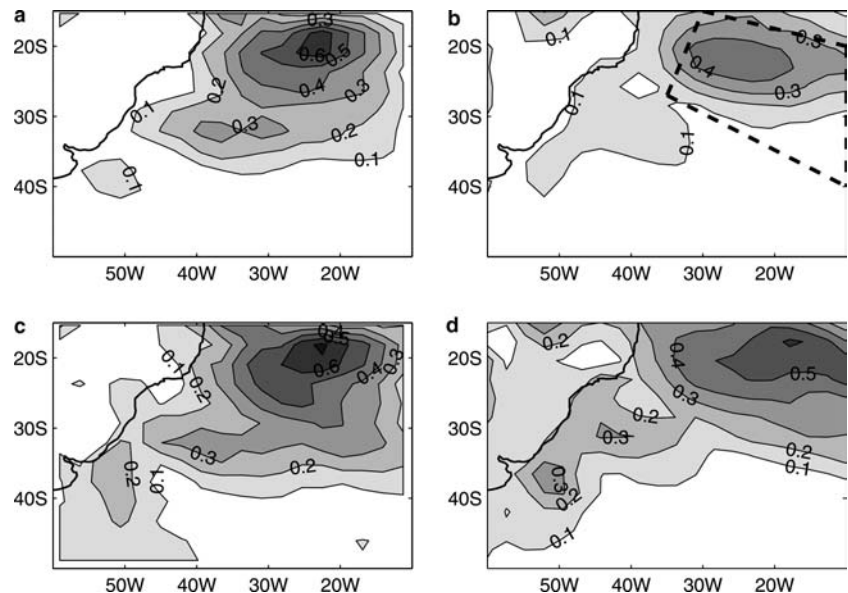
slightly different season considered. Nevertheless, ANOVA estimates are larger for both models, particularly for the NSIPP-1, showing that PP gives a conservative estimate of the potential predictability.

Figure 7 indicates that over the ocean the predictable variance has a maximum value of about 60% of total variability, but the mean over the ocean is considerably smaller than that. This suggests that the variability in the SACZ region is dominated by the internal atmospheric variability (and land-surface variability) in agreement with previous estimates of BCS and with results of Robertson and Mechoso (2000). The signal variance accounts for a relatively large portion of the total variance only in the positive lobe of the forced precipitation dipole pattern, and the maximum is shifted further away from the coast, compared with Fig. 3a, b. The reason is the extension of the noise variance into the oceanic region weakening the PP next to the coast (see also Fig. 6).

The results above suggest that the ocean surface is a source of potential predictability to the oceanic portion of the SACZ. Also, they indicate that it is in that region, that the forced signal shown in Fig. 3 is likely to be an important player in the dynamics. These results, however, are derived based on ensembles of model simulations and do not directly address the issue of how skillful these models are in simulating/predicting rainfall observed in the region on interannual timescales. To address this issue, we constructed a precipitation index as an average over the area shown in Fig. 7b. The choice of the area is based on the criterion that the forced variance must explain at least 30% of the total variance in both models. The southern limit is defined by the axis of the forced precipitation dipole (see Fig. 3b). Also, note that the area follows the shape of the positive lobe in the precipitation dipole and that it contains the region of maximum amplitude.

Figure 8 shows the index for the observational data set (dashed line) together with the time series of the

Fig. 7 Estimates of potential predictability given by the PP index for **a** CCM3 and **b** NSIPP-1 models; and given by ANOVA for **c** CCM3 and **d** NSIPP-1 models. For ANOVA estimates, contours larger than 0.1 are significant at the 99% level. The *dashed box* in **(b)** marks the region used to construct the precipitation index shown in Fig. 8



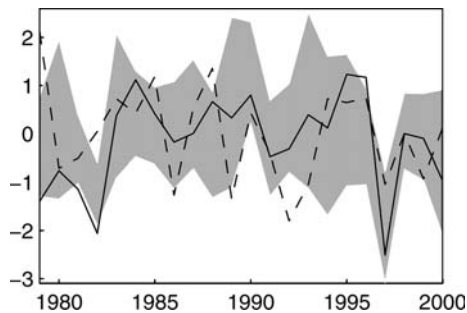


Fig. 8 Time series of forced response in NSIPP-1 model (solid line) and time series of the precipitation index in the observations (dashed line). Shading shows the dispersion of the index for precipitation calculated for all NSIPP-1 ensemble members (see text).

forced response for the NSIPP-1 model (solid line, same as in Fig. 3c). The shaded region denotes the dispersion of the precipitation index calculated for the ensemble members. As expected, due to the relatively large noise variance in the region, the index shows large intra-ensemble dispersion. Note that the dispersion interval almost always contains the time series of the forced response. The index for the observations also generally lies within the dispersion of the ensemble members, suggesting that the model simulates well the precipitation variability in the region. Moreover, the precipitation index that was observed shows a correlation of 0.45 with the time series of the forced response during the period 1980–2000, which is significant at the 95% level. These results suggest that the forced response of the precipitation to SST anomalies is present not only in the models, but also in the real world. However, this also suggests that the forced signal is weak and its manifestation is confined to oceanic regions away from the coast where the internal variability is relatively weak compared to that over the land region.

6 Summary and discussion

The output of two state of the art AGCMs is analyzed using a technique devised for separating signal from noise under the assumption of additivity. The models include different physical packages for convective parameterizations, soil moisture feedbacks and land representations that led to different overall interannual precipitation variability in the SACZ region (Fig. 2b, d). Nevertheless, the models consistently show a very similar forced precipitation signal mainly in the oceanic part of the SACZ, which does not extend very much into the continent. The signal has interannual-to-decadal timescales and consists of a shift and strengthening of the SACZ towards anomalously warm waters present over most of the South Atlantic basin between 0 and 30°S. Our results, together with those of Robertson et al. (2003), suggest that the pattern of atmospheric response in the SACZ region to Atlantic SST anomalies is very robust.

In the SACZ region, the behavior of the heat fluxes associated with the forced response is somewhat different in the models. While in the NSIPP-1 heat fluxes tend to damp the SST anomalies, in the CCM3 there is a region next to the coast of Brazil where positive heat-flux anomalies coexist with warm SST anomalies, thus indicating the existence of a positive air–sea feedback. On the other hand, both models suggest the existence of a region of positive feedback off the coast of Brazil at about 10°S.

How important is the signal compared to the background noise? A potential predictability analysis performed for the two GCMs indicates that the SACZ region is largely dominated by internal variability. The forced component is present only over the ocean where it explains a maximum of about 50% of total variability. Accordingly, over the continent we expect the noise-EOF1 to be the dominant player. The manifestation of the forced signal is seen further away from the coast than Fig. 3a, b tends to suggest, due to the extension of large internal variability into the ocean. An analysis on the observational rainfall record suggests that the signal also exists in the real atmosphere.

The leading mode of internal variability on interannual timescales (noise-EOF1) shows an enhanced SACZ accompanied by decreased rainfall over southern Brazil, Uruguay and northern Argentina (or vice versa). This structure is very similar to the leading pattern of observed vertical velocity found by Robertson and Mechoso (2000) in the SACZ region on interannual timescales, reinforcing the conclusion that the SACZ is dominated by internal variability. Interestingly, a similar pattern was also found in observations as the leading mode of variability on intraseasonal timescales (Paegle et al. 2000).

In summary, results show that the continental part of the SACZ has very limited predictability associated with SST variations. Accordingly, the best hope for prediction beyond the 1–2-weeks limit imposed by the chaotic atmospheric dynamics may rely on the foreknowledge of the land surface moisture state (Koster et al. 2000). The coastal region may still have some predictability associated to SST anomalies. Rainfall over southern Brazil and Uruguay might also have added predictability by means of the moisture flux associated with the South American Low-Level Jet (Marengo et al. 2004). These issues need to be addressed using regional high-resolution models with improved land physics and convective parameterizations. Finally, models suggest that there is substantial oceanic forcing of the atmosphere in the subtropics (Fig. 7), an area where atmosphere–ocean coupling has not been explored much (in contrast to equatorial regions) and that deserves future attention.

Acknowledgements Marcelo Barreiro would like to thank Roberto Mechoso, Alessandra Giannini and John Chiang for a very useful discussions and comments. Marcelo Barreiro was supported by NASA Headquarters under the Earth System Science Fellowship Grant NGT5-30417. This work was partially supported by NASA InterAgency Agreement W-19,750 and by NOAA Grant NA16GP1575.

References

- Arakawa A, Schubert WH (1974) Interaction of a cumulus cloud ensemble with the large-scale environment, part I. *J Atmos Sci* 31:674–701
- Bacmeister JT, Pegion PJ, Schubert SD, Suarez MJ (2000) Atlas of seasonal means simulated by the NSIPP-1 atmospheric GCM. NASA Technical Memorandum 104606, vol 17, p 194
- Barreiro M, Chang P, Saravanan R (2002) Variability of the South Atlantic convergence zone as simulated by an atmospheric general circulation model. *J Climate* 15:745–763
- Bonan GB (1998) The land surface climatology of the NCAR Land Surface Model coupled to the NCAR Community Climate Model. *J Climate* 11:1307–1326
- Chang P, Saravanan R, Ji L, Hegerl GC (2000) The effect of local sea surface temperature on atmospheric circulation over the tropical Atlantic sector. *J Climate* 13:2195–2216
- Gill A (1980) Some simple solutions for heat-induced tropical circulation. *Q J R Meteorol Soc* 106:447–462
- Goddard L, Mason SJ, Zebiak SE, Ropelewsky CF, Basher R, Cane MA (2001) Current approaches to seasonal-to-interannual climate predictions. *Int J Climatol* 21:1111–1152
- Hack JJ (1994) Parameterization of moist convection in the National Center for Atmospheric Research community climate model (CCM2). *J Geophys Res* 99:5551–5568
- Hack JJ, Kiehl JT, Hurrell JW (1998) The hydrology and thermodynamic characteristics of the NCAR CCM3. *J Climate* 11:1179–1206
- Huffman GJ, Adler RF, Arkin P, Chang A, Ferraro R, Gruber A, Janowiak J, McNab A, Rudolf B, Schneider U (1997) The Global Precipitation Climatology project (GPCP) combined precipitation dataset. *Bull Am Meteorol Soc* 78:5–20
- Kiehl JT, Hack JJ, Bonan GB, Boville BP, Williamson DL, Rasch PJ (1998) The National Center for Atmospheric Research Community Climate Model: CCM3. *J Climate* 11:1131–1149
- Kodama Y-M (1992) Large scale common features of subtropical precipitation zones (the Baiu frontal zone, the SPCZ and the SACZ) Part I: Characteristics of subtropical frontal zones. *J Meteor Soc Japan* 70:813–836
- Kodama Y-M (1993) Large scale common features of subtropical precipitation zones (the Baiu frontal zone, the SPCZ and the SACZ) Part II: Conditions of the circulations for generating the STCZs. *J Meteor Japan* 71:581–610
- Koster RD, Suarez MJ (1996) Energy and water balance calculations in the Mosaic LSM. NASA Technical Memorandum no. 104606, vol 9, p 58
- Koster RD, Suarez MJ, Heiser M (2000), Variance and predictability of precipitation at seasonal-to-interannual timescales. *J Hydrometeorol* 1:26–46
- Liebmann B, Kiladis GN, Marengo JA, Ambrizzi T, Glick JD (1999) Submonthly convective variability over South America and the South Atlantic convergence zone. *J Climate* 12:1877–1891
- Marengo JA, Soares WR, Saulo C, Nicolini M (2004) Climatology of the low-level jet east of the Andes as derived from the NCEP-NCAR reanalysis: Characteristics and temporal variability. *J Climate* 17:2261–2280
- Moorthi S, Suarez MJ (1992) Relaxed Arakawa-Shubert: a parameterization of moist convection for general circulation models. *Mon Wea Rev* 120:978–1002
- Paegle JN, Byerle LA, Mo KC (2000) Intraseasonal modulation of South American summer precipitation. *Mon Wea Rev* 128:837–850
- Rayner NA, Horton EB, Parker DE, Folland CK, Hackett RB (1996) Version 2.2 of the global sea-ice and sea surface temperature data set, 1931–1994. Climate Research Technical Note 74, Hadley Centre, Meteorological Office, Bracknell, United Kingdom. [Available from Hadley Centre, London Rd., Bracknell, Berkshire RG12 2SY, United Kingdom]
- Reynolds RW, Smith TM (1994) Improved global sea surface temperature analyzes using optimum interpolation. *J Climate* 7:929–948
- Robertson AW, Mechoso CR (2000) Interannual and decadal variability of the South Atlantic convergence zone. *Mon Wea Rev* 128:2947–2957
- Robertson AW, Mechoso CR, Kim Y-J (2000) The influence of Atlantic sea surface temperature anomalies on the North Atlantic Oscillation. *J Climate* 13:122–138
- Robertson AW, Farrara JD, Mechoso CR (2003) Simulations of the atmospheric response to South Atlantic sea surface temperature anomalies. *J Climate* 16:2540–2551
- Rowell DP (1998) Assessing potential seasonal predictability with an ensemble of multidecadal GCM simulations. *J Climate* 11:109–120
- Saravanan R (1998) Atmospheric low-frequency variability and its relationship to midlatitude SST variability: studies using the NCAR climate system model. *J Climate* 11:1386–1404
- Saravanan R, Chang P (2000) Interaction between tropical Atlantic variability and El Niño-Southern oscillation. *J Climate* 13:2177–2194
- Smith TM, Reynolds RW, Livezey RE, Stokes DC (1996) Reconstruction of historical sea surface temperatures using empirical orthogonal functions. *J Climate* 9:1403–1420
- Sterl A, Hazeleger W (2003) Coupled variability and air-sea interaction in the South Atlantic Ocean. *Climate Dynam* 21:559–571
- von Storch H, Zwiers F (1999) Statistical analysis in climate research. Cambridge University Press, London, p 484
- Venzke S, Allen MR, Sutton RT, Rowell DP (1999) The atmospheric response over the North Atlantic to decadal changes in sea surface temperature. *J Climate* 12:2562–2584
- Zhang GJ, McFarlane NA (1995) Sensitivity of climate simulations to the parameterization of cumulus convection in the Canadian Climate Centre general circulation model. *Atmos Ocean* 33:407–446